catalysts

MDPI

Article

Improving Catalytic Activity towards the Direct Synthesis of H_2O_2 through Cu Incorporation into AuPd Catalysts

Alexandra Barnes [1,†], Richard J. Lewis [1,*,†], David J. Morgan [1,2], Thomas E. Davies [1] and Graham J. Hutchings [1,*]

[1] Max Planck-Cardiff Centre on the Fundamentals of Heterogeneous Catalysis FUNCAT, Cardiff Catalysis Institute, School of Chemistry, Cardiff University, Main Building, Park Place, Cardiff CF10 3AT, UK
[2] Harwell XPS, Research Complex at Harwell (RCaH), Didcot OX11 0FA, UK
* Correspondence: lewisr27@cardiff.ac.uk (R.J.L.); hutch@cardiff.ac.uk (G.J.H.)
† These authors contributed equally to this work.

Abstract: With a focus on catalysts prepared by an excess-chloride wet impregnation procedure and supported on the zeolite ZSM-5(30), the introduction of low concentrations of tertiary base metals, in particular Cu, into supported AuPd nanoparticles can be observed to enhance catalytic activity towards the direct synthesis of H_2O_2. Indeed the optimal catalyst formulation ($1\%AuPd_{(0.975)}Cu_{(0.025)}$/ZSM-5) is able to achieve rates of H_2O_2 synthesis (115 $mol_{H_2O_2} kg_{cat}^{-1} h^{-1}$) approximately 1.7 times that of the bi-metallic analogue (69 $mol_{H_2O_2} kg_{cat}^{-1} h^{-1}$) and rival that previously reported over comparable materials which use Pt as a dopant. Notably, the introduction of Cu at higher loadings results in an inhibition of performance. Detailed analysis by CO-DRFITS and XPS reveals that the improved performance observed over the optimal catalyst can be attributed to the electronic modification of the Pd species and the formation of domains of a mixed Pd^{2+}/Pd^0 oxidation state as well as structural changed within the nanoalloy.

Keywords: hydrogen peroxide; gold; palladium; copper; trimetallic; green chemistry

Citation: Barnes, A.; Lewis, R.J.; Morgan, D.J.; Davies, T.E.; Hutchings, G.J. Improving Catalytic Activity towards the Direct Synthesis of H_2O_2 through Cu Incorporation into AuPd Catalysts. *Catalysts* **2022**, *12*, 1396. https://doi.org/10.3390/catal12111396

Academic Editor: Carl Redshaw

Received: 18 October 2022
Accepted: 2 November 2022
Published: 9 November 2022

1. Introduction

The direct synthesis of H_2O_2 from molecular H_2 and O_2 (Scheme 1) represents an attractive alternative to the current means of large-scale production of this environmentally benign, powerful oxidant, the anthraquinone oxidation (AO) process. Indeed, the direct approach would allow for the production of appropriate concentrations of H_2O_2 at the point of final use, avoiding the substantial economic and environmental drawbacks associated with the industrial route. Due to production costs, H_2O_2 production via the AO process is typically centralised, with H_2O_2 transported at concentrations in excess of that required by the end-user [1]. The subsequent dilution of the oxidant prior to use effectively wastes a significant amount of energy associated with the initial purification and concentration steps [2]. Additionally, H_2O_2 is relatively unstable, decomposing readily to H_2O in the presence of mild temperatures or weak bases and, as such, requires acid stabilizers to prolong its shelf-life [3], which results in complex product streams and can deleteriously affect the reactor lifetime [4]. These cumulative drawbacks associated with off-site H_2O_2 production pass on significant costs to the end user, which would be greatly reduced or removed altogether via a direct synthesis approach to H_2O_2 production. In particular, the direct route may find the greatest application for oxidative transformations where the synthesised H_2O_2 is readily utilised for chemical valorisation or generated in situ [5–7].

A Langmuir–Hinshelwood mechanism involving the successive hydrogenation of molecular O_2 has been often proposed for the direct synthesis reaction [8,9]. However, in recent years Flaherty and co-workers have advanced an alternative, non-Langmuirian

mechanism [10], which involves a water-mediated proton-electron transfer and have further reported the role of protic solvents in the formation of surface-bound intermediates that shuttle both the protons and electrons to active sites [11]. Indeed, detailed theoretical studies have further demonstrated that energy barriers associated with a solvent-mediated protonation of adsorbed O_2 are not prohibitive and, indeed, are as low as O_2 hydrogenation [12].

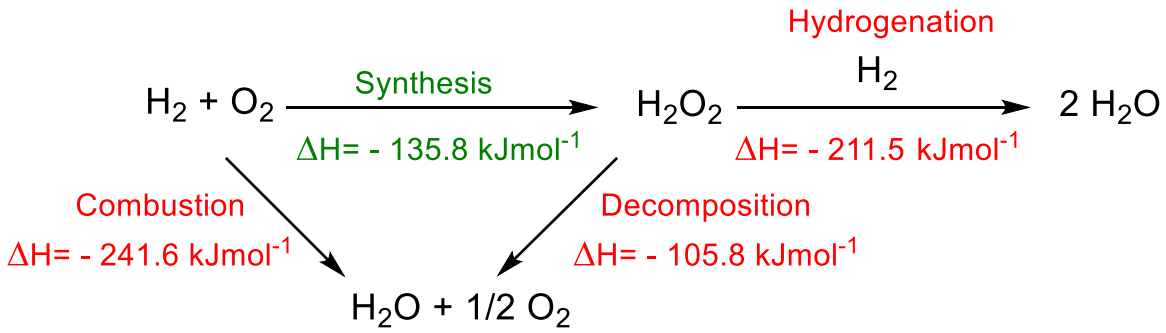

Scheme 1. Reaction pathways associated with the direct synthesis of H_2O_2 from H_2 and O_2.

Pd-based catalysts have been well studied for their application in the direct synthesis reaction [13–15] since the first patent was granted to Henkel and Weber in 1914 [16]. However, a major challenge associated with catalytic selectivity has prevented the development of an industrial-scale direct synthesis process [17,18]. This can be understood as the formation of H_2O is thermodynamically more favourable than that of H_2O_2, with H_2O formation driven via combustion or through the subsequent degradation of H_2O_2 (via decomposition and hydrogenation pathways).

Measures to improve catalytic selectivity have often focused on the introduction of secondary metals into supported Pd catalysts, with AuPd systems being perhaps the most extensively studied [19–21]. In recent years, significant attention has been placed on the alloying of Pd with a range of earth-abundant metals [22–27]. Further investigations have focused on the introduction of dopant levels of precious metals, such as Pt, into supported Pd [28–33] and AuPd [34–37] catalysts. The resulting improved catalytic activity towards H_2O_2 production is often attributed to a combination of the electronic promotion of Pd and the isolation of contiguous Pd domains, widely considered to be key in promoting the cleavage of O–O bonds (in $*O_2$, $*H_2O_2$, or *OOH) and the resultant formation of H_2O [38–40].

The use of zeolitic and zeo-type materials as catalyst supports for use in the direct synthesis of H_2O_2 has received significant attention, with such catalysts typically offering improved activity and selectivity compared to oxide-supported analogues [5,36,41–43]. This has often been attributed to the improved dispersion of metal species and the acidic nature of the support materials, with supports of low isoelectric points (i.e., the pH at which the surface has zero net charges and an indication of catalyst acidity/basicity) and are reported to offer enhanced catalytic performance compared to those with a high isoelectric point [20].

Recently, we have demonstrated that significant improvements in catalytic performances can be achieved through the introduction of low concentrations of base metals into AuPd nanoalloys when supported on TiO_2 (P25) [44]. Indeed, the catalysts developed within this earlier work offered comparable H_2O_2 synthesis rates to those previously observed through Pt incorporation while avoiding the additional cost associated with the precious metal dopant [44]. With these earlier studies in mind, we now investigate the efficacy of base metal-incorporated AuPd catalysts supported on the zeolite ZSM-5(30) towards the direct synthesis of H_2O_2.

2. Experimental Section

2.1. Catalyst Preparation

Prior to the co-impregnation of metal salts, the NH_4-ZSM-5 material (SiO_2:Al_2O_3 = 30:1, Alfa Aesar) was calcined (flowing air, 550 °C, 3 h, 20 °C min^{-1}).

A series of bi- and tri-metallic 1%AuPdX/ZSM-5 (X = Cu, Ni, Zn) catalysts were prepared by an excess chloride wet co-impregnation procedure, based on the methodology previously reported in the literature, which has been shown to result in the enhanced dispersion of precious metals, in particular Au, when compared to conventional wet co-impregnation methodologies [45]. The procedure to produce $1\%AuPd_{(0.975)}Cu_{(0.025)}$/ZSM-5 (1 g) is outlined below where the total metal loading was 1 wt.%, the combined weight loading of Au and Pd was 0.975 wt.%, and that of Cu was 0.025 wt.%, and in all cases the Au:Pd ratio was 1:1 (mol/mol). A similar methodology to that outlined below was utilised for all catalysts investigated, with the exact quantities of metal precursor used to synthesise the key catalysts used within this work reported in Table S1.

Aqueous solutions of $HAuCl_4.3H_2O$ (0.322 mL, 12.25 $mgmL^{-1}$, Strem Chemicals), $PdCl_2$ (0.356 mL, 6 $mgmL^{-1}$, 0.58 M HCl, Sigma Aldrich, Burlington, MA, USA), and $CuCl_2$ (106 µL, 2.36 $mgmL^{-1}$, Sigma Aldrich) were mixed in a 50 mL round bottom flask and heated to 60 °C with stirring (1000 rpm) in a thermostatically controlled oil bath, with the total volume fixed to 16 mL using H_2O (HPLC grade). Upon reaching 65 °C, ZSM-5 (0.99 g, SiO_2:Al_2O_3 = 30:1, Alfa Aesar) was added over the course of 10 min with constant stirring. The resultant slurry was stirred at 60 °C for a further 15 min, and following this, the temperature was raised to 95 °C for 16 h to allow for the complete evaporation of water. The resulting solid was ground prior to heat treatment in a reductive atmosphere ($5\%H_2$/Ar, 400 °C, 4 h, 10 °Cmin^{-1}).

2.2. Catalyst Testing

Note 1. *Reaction conditions used within this study operate under the flammability limits of gaseous mixtures of H_2 and O_2.*

Note 2. *The conditions used within this work for H_2O_2 synthesis and degradation have previously been investigated, with the presence of CO_2 as a diluent for reactant gases and a methanol co-solvent being identified as key to maintaining high catalytic efficacy towards H_2O_2 production [45]. In regard to the role of the CO_2 diluent, this was found to act as an in-situ promoter of H_2O_2 stability through its dissolution in the reaction solution and the formation of carbonic acid. We have previously reported that the use of the CO_2 diluent has a comparable promotive effect to that observed when acidifying the reaction solution to a pH of 4 using HNO_3 [46].*

2.3. Direct Synthesis of H_2O_2

Hydrogen peroxide synthesis was evaluated using a Parr Instruments stainless steel autoclave with a nominal volume of 100 mL, equipped with a PTFE liner so that the total volume was reduced to 66 mL and a maximum working pressure of 2000 psi. To test each catalyst for H_2O_2 synthesis, the autoclave liner was charged with a catalyst (0.01 g), solvent (methanol (5.6 g, HPLC grade, Fischer Scientific, Waltham, MA, USA), and H_2O (2.9 g, HPLC grade, Fischer Scientific)). The charged autoclave was then purged three times with $5\%H_2/CO_2$ (100 psi) before filling with $5\%H_2/CO_2$ to a pressure of 420 psi, followed by the addition of $25\%O_2/CO_2$ (160 psi), with the pressure of $5\%H_2/CO_2$ and $25\%O_2/CO_2$ given as gauge pressures. The reactor was not continually fed with reactant gas. The reaction was conducted at a temperature of 2 °C for 0.5 h with stirring (1200 rpm). The H_2O_2 productivity was determined by titrating aliquots of the final solution after the reaction with acidified $Ce(SO_4)_2$ (0.0085 M) in the presence of a ferroin indicator. Catalyst productivities are reported as $mol_{H_2O_2}kg_{cat}^{-1}h^{-1}$.

The catalytic conversion of H_2 and selectivity towards H_2O_2 were determined using a Varian 3800 GC fitted with TCD and equipped with a Porapak Q column.

H_2 conversion (Equation (1)) and H_2O_2 selectivity (Equation (2)) are defined as follows:

$$H_2\text{Conversion}\ (\%) = \frac{\text{mmol}_{\text{H2 (t(0))}} - \text{mmol}_{\text{H2 (t(1))}}}{\text{mmol}_{\text{H2 (t(0))}}} \times 100 \quad (1)$$

$$H_2O_2\ \text{Selectivity}\ (\%) = \frac{H_2O_2\text{detected (mmol)}}{H_2\ \text{consumed (mmol)}} \times 100 \quad (2)$$

The total autoclave capacity was determined via water displacement to allow for the accurate determination of H_2 conversion and H_2O_2 selectivity. When equipped with the PTFE liner, the total volume of an unfilled autoclave was determined to be 93 mL, which included all available gaseous space within the autoclave.

2.4. Gas Replacement Experiments for the Direct Synthesis of H_2O_2

An identical procedure to that outlined above for the direct synthesis reaction was followed for a reaction time of 0.5 h. After this, stirring was stopped, and the reactant gas mixture was vented prior to replacement with the standard pressures of 5% H_2/CO_2 (420 psi) and 25% O_2/CO_2 (160 psi). The reaction mixture was then stirred (1200 rpm) for a further 0.5 h. To collect a series of data points, as in the case of Figure 5, it should be noted that individual experiments were carried out, and the reactant mixture was not sampled online.

2.5. Catalyst Reusability in the Direct Synthesis and Degradation of H_2O_2

In order to determine catalyst reusability, a similar procedure to that outlined above for the direct synthesis of H_2O_2 was followed utilising 0.05 g of catalyst. Following the initial test, the catalyst was recovered by filtration and dried (30 °C, 16 h, under vacuum); from the recovered catalyst sample 0.01 g and was used to conduct a standard H_2O_2 synthesis or degradation test.

2.6. Degradation of H_2O_2

Catalytic activity towards H_2O_2 degradation was determined in a similar manner to the direct synthesis activity of a catalyst. The autoclave liner was charged with a solvent (methanol (5.6 g, HPLC grade, Fischer Scientific), H_2O (2.9 g, HPLC grade, Fischer Scientific)), and H_2O_2 (50 wt. % 0.69 g, Sigma Aldrich), with the resultant solvent composition equivalent to a 4 wt. % H_2O_2 solution. From the solution, two 0.05 g aliquots were removed and titrated with acidified $Ce(SO_4)_2$ solution using ferroin as an indicator to determine an accurate concentration of H_2O_2 at the start of the reaction. Subsequently, a catalyst (0.01 g) was added to the reaction media, and the autoclave was purged with 5%H_2/CO_2 (100 psi) prior to being pressurised with 5%H_2/CO_2 (420 psi). The reaction medium was cooled to a temperature of 2 °C prior to stirring (1200 rpm) for 0.5 h. After the reaction was complete, the catalyst was removed from the reaction mixture, and two 0.05 g aliquots were titrated against the acidified $Ce(SO_4)_2$ solution using ferroin as an indicator. The degradation activity is reported as $\text{mol}_{H_2O_2}\text{kg}_{\text{cat}}{}^{-1}\text{h}^{-1}$.

Note 3. *In all cases, the reactor temperature was controlled using a HAAKE K50 bath/circulator and an appropriate coolant. The reactor temperature was maintained at 2 ± 0.2 °C throughout the course of the H_2O_2 synthesis and degradation reaction.*

In all cases, the reactions were run multiple times, over multiple batches of catalysts, with the data being presented as an average of these experiments. The catalytic activity toward the direct synthesis and subsequent degradation of H_2O_2 was found to be consistent to within ±3% on the basis of multiple reactions.

2.7. Characterisation

A Thermo Scientific K-Alpha$^+$ photoelectron spectrometer was used to collect XP spectra utilising a micro-focused monochromatic Al K_α X-ray source operating at 72 W.

Samples were pressed into a copper holder and analysed using the 400 μm spot mode at pass energies of 40 and 150 eV for high-resolution and survey spectra, respectively. Charge compensation was performed using a combination of low-energy electrons and argon ions, which resulted in a C(1s) binding energy of 284.8 eV for the adventitious carbon present in all the samples and all samples also showed a constant Ti($2p_{3/2}$) of 458.5 eV. All data were processed using CasaXPS v2.3.24 (Casa Software Ltd., Teignmouth, UK) with a Shirley background, Scofield sensitivity factors, and an electron energy dependence of −0.6, as recommended by the manufacturer. Peak fits were performed using a combination of Voigt-type functions and models derived from the bulk reference samples where appropriate.

The bulk structure of the catalysts was determined by powder X-ray diffraction using a (θ-θ) PANalytical X'pert Pro powder diffractometer with a Cu K_α radiation source, operating at between 40 keV and 40 mA. Standard analysis was carried out using a 40 min run with a backfilled sample, between 2θ values of 5 and 75°. Phase identification was carried out using the International Centre for Diffraction Data (ICDD).

Note 4. *X-ray diffractograms of key as-prepared catalysts are reported in Figure S1 (and accompanying text) with no reflections associated with active metals, indicative of the relatively low total loading and high dispersion of the immobilised metals.*

Transmission electron microscopy (TEM) was performed on a JEOL JEM-2100 (Tokyo, Japan) operating at 200 kV. Samples were prepared through their dispersion in ethanol by sonication, and they were deposited on 300 mesh copper grids coated with holey carbon film. Energy dispersive X-ray spectroscopy (XEDS) was performed using an Oxford Instruments (Abingdon, UK) X-Max^N 80 detector, and the data analysed used Aztec software (Abingdon, UK). Aberration corrected scanning transmission electron microscopy (AC-STEM) was performed using a probe-corrected Hitachi (Brisbane, Australia) HF5000 S/TEM, operating at 200 kV. The instrument was equipped with bright field (BF), high angle annular dark field (HAADF), and secondary electron (SE) detectors for high spatial resolution STEM imaging experiments. This microscope was also equipped with a secondary electron detector and dual Oxford Instruments (Abingdon, UK) XEDS detectors (2×100 mm^2) with a total collection angle of 2.02 sr.

Total metal leaching from the supported catalyst was quantified via inductively coupled plasma mass spectrometry (ICP-MS). Post-reaction solutions were analysed using an Agilent (Santa Clara, CA, USA) 7900 ICP-MS equipped with an I-AS auto-sampler. All samples were diluted by a factor of 10 using HPLC grade H_2O (1%HNO_3 and 0.5% HCl matrix). All calibrants were matrix matched and measured against a five-point calibration using certified reference materials purchased from Perkin Elmer and certified internal standards acquired from Agilent.

Fourier-transform infrared spectroscopy (FTIR) was carried out with a Bruker (Hanau, Germany) Tensor 27 spectrometer fitted with a HgCdTe (MCT) detector and was operated with OPUS software (Ettinger, Germany).

Note 5. *FTIR analysis of key as-prepared catalysts is reported in Figure S2 (and accompanying text) and indicates no discernible changes in the structure of the HZSM-5 support upon metal immobilisation and exposure to a reductive heat treatment.*

N_2 isotherms were collected on a Micromeritics 3-Flex. Samples (ca. 0.070 g) were degassed (350 °C, 9 h) prior to analysis. Analyses were carried out at 77 K, with P_0 measured continuously. Free space was measured post-analysis with He. Data analyses were carried out using the Micromeritics 3-Flex software with the non-local density functional theory (NLDFT), Tarazona model.

Note 6. *The details of the textural properties of key ZSM-5-supported catalysts are reported in Table S2 and Figure S3. The immobilisation of active metals can be seen to lead to a general decrease in both the total surface area and pore volume in comparison to the bare ZSM-5 support. This is ascribed to the deposition of metal nanoparticles inside the zeolitic pore structure.*

3. Results and Discussion

The introduction of small concentrations of precious dopants, in particular Pt, [38,39] into the supported AuPd nanoalloys has been extensively reported to offer improved catalytic activity towards the direct synthesis of H_2O_2, when compared to the bimetallic analogue. We recently demonstrated that comparable enhancements in performance could result from the incorporation of dopant concentrations of base meals into AuPd nanoalloys [44]. In keeping with this earlier work, our initial investigations identified the promotive effect that can result from the introduction of Cu, Ni, and Zn at low concentrations (0.025 wt.%) into a $1\%AuPd_{(1.00)}/ZSM\text{-}5$ catalyst (Figure 1). In particular, the introduction of Cu, which is known to be readily incorporated into AuPd alloys [47], was observed to significantly increase activity towards H_2O_2 synthesis, with this metric approximately 1.7 times greater (115 $mol_{H_2O_2}kg_{cat}^{-1}h^{-1}$), than that observed for the bi-metallic $1\%AuPd_{(1.00)}/ZSM\text{-}5$ catalyst (69 $mol_{H_2O_2}kg_{cat}^{-1}h^{-1}$). Indeed, the activity of the $1\%AuPd_{(0.975)}Cu_{(0.025)}/ZSM\text{-}5$ catalyst exceeded that of the analogous formulation supported on TiO_2 (P25) (94 $mol_{H_2O_2}kg_{cat}^{-1}h^{-1}$) [44]. However, a concurrent increase in catalytic activity towards the subsequent degradation of H_2O_2 (via decomposition and hydrogenation pathways) was also observed (529 $mol_{H_2O_2}kg_{cat}^{-1}h^{-1}$). This may be surprising given earlier works which have demonstrated that the addition of Cu, either into AuPd [48] or Pd-only [49] catalysts, can inhibit catalytic activity, with DFT studies indicating that the formation of the intermediate hydroperoxyl species (OOH*) and subsequently H_2O_2 is thermodynamically unfavoured over Cu-containing precious metal surfaces [50]. However, notably, these prior works have focused on the incorporation of Cu at much higher concentrations than that utilised within this study. In comparison, the introduction of Ni (81 $mol_{H_2O_2}kg_{cat}^{-1}h^{-1}$) and Zn (77 $mol_{H_2O_2}kg_{cat}^{-1}h^{-1}$) resulted in only a minor improvement in the catalyst performance compared to the bi-metallic AuPd analogue, although the improved selectivity of the $1\%AuPd_{(0.975)}Ni_{(0.025)}/ZSM\text{-}5$ catalyst is noteworthy, with H_2O_2 degradation rates (281 $mol_{H_2O_2}kg_{cat}^{-1}h^{-1}$) significantly lower than that observed over the $1\%AuPd_{(1.00)}/ZSM\text{-}5$ catalyst (320 $mol_{H_2O_2}kg_{cat}^{-1}h^{-1}$) or, indeed, the other trimetallic formulations. The enhanced performance of the $1\%AuPd_{(0.975)}Cu_{(0.025)}/ZSM\text{-}5$ catalyst is further evidenced by the comparison of initial reaction rates, where the contribution of competitive H_2O_2 degradation pathways is considered to be negligible (Table S3).

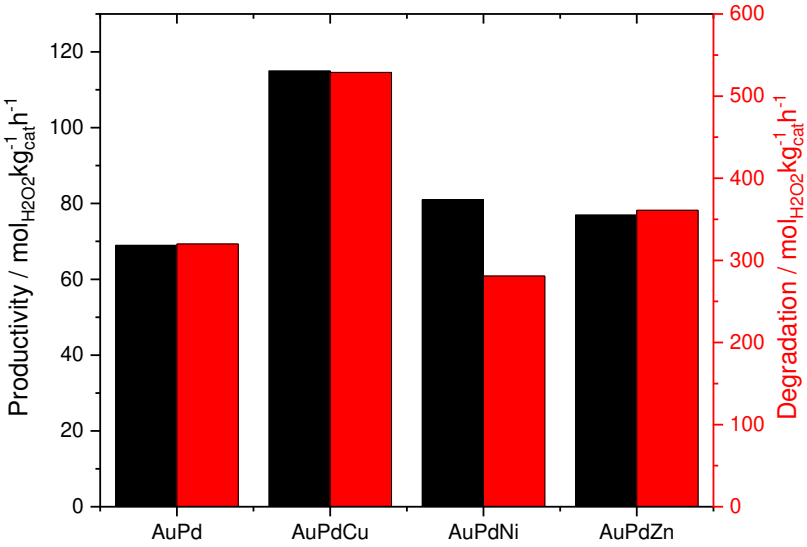

Figure 1. Catalytic activity towards $1\%AuPd_{(0.975)}X_{(0.025)}/ZSM\text{-}5$, the direct synthesis, and subsequent degradation of H_2O_2. **H_2O_2 direct synthesis reaction conditions:** catalyst (0.01 g), H_2O (2.9 g), MeOH (5.6 g), 5% H_2/CO_2 (420 psi), 25% O_2/CO_2 (160 psi), 0.5 h, 2 °C, and 1200 rpm. **H_2O_2 degradation reaction conditions:** catalyst (0.01 g), H_2O_2 (50 wt.% 0.68 g) H_2O (2.22 g), MeOH (5.6 g), 5% H_2/CO_2 (420 psi), 0.5 h, 2 °C, and 1200 rpm.

An evaluation of the as-prepared 1%$AuPd_{(0.975)}X_{(0.025)}$/ZSM-5 catalysts by XPS can be seen in Figure 2 (additional data reported in Table S4). Interestingly, despite exposure to a high-temperature reductive heat treatment (5%H_2/Ar, 400 °C, 4 h, 10 °Cmin^{-1}), the 1%$AuPd_{(1.00)}$/ZSM-5 catalyst was found to consist of a relatively high proportion of Pd^{2+}. Such an observation is in keeping with our previous investigations into AuPd systems, where the introduction of Au has been found to modify Pd speciation [20]. Upon the introduction of low quantities of Ni, Cu, and Zn, a significant shift in Pd speciation was observed, towards Pd^{2+}, with the formation of mixed domains of the Pd oxidation state, which is well known to offer improved activity compared to Pd^0 or Pd^{2+} rich analogues [51]. The shift in the Pd oxidation state towards Pd^{2+} upon the introduction of Ni was found to be the greatest, which aligned well with the observed selectivity of the 1%$AuPd_{(0.975)}Ni_{(0.025)}$/ZSM-5 catalyst. However, it should be noted that the Pd speciation of the fresh catalyst is likely to be not representative of those under direct synthesis reaction conditions.

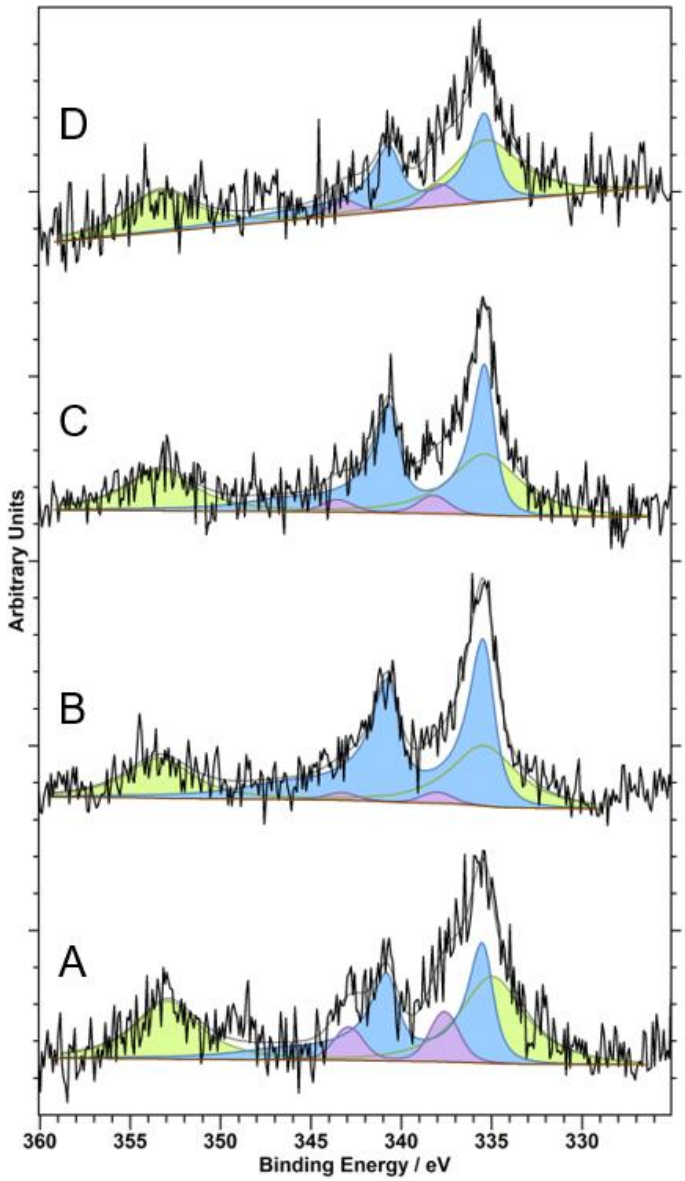

Figure 2. XPS spectra of Pd(3d) regions for the as-prepared 1%$AuPd_{(0.975)}X_{(0.025)}$/ZSM-5 catalysts as a function of tertiary metal dopant. (**A**) 1%$AuPd_{(1.00)}$/ZSM-5; (**B**) 1%$AuPd_{(0.975)}Cu_{(0.025)}$/ZSM-5; (**C**) 1%$AuPd_{(0.975)}Ni_{(0.025)}$/ZSM-5; and (**D**) 1%$AuPd_{(0.975)}Zn_{(0.025)}$/ZSM-5. ***Key:*** Au(4d) (green); Pd^0(blue); Pd^{2+}(purple).

With the improved activity of the 1%AuPd$_{(0.975)}$Cu$_{(0.025)}$/ZSM-5 catalyst towards H_2O_2 production established, we were subsequently motivated to determine the effect of Cu loading on catalytic activity while maintaining the total metal loading at 1 wt.% (Figure 3A,B, with initial reaction rates reported in Table S5). The introduction of low concentrations of Cu (< 0.025 wt.%) was observed to significantly increase the catalytic activity towards both the direct synthesis and subsequent degradation of H_2O_2, compared to the bimetallic AuPd parent material. However, both these metrics decreased considerably at higher loadings of Cu (75 and 287 $mol_{H_2O_2}kg_{cat}^{-1}h^{-1}$, respectively, for H_2O_2 direct synthesis and degradation pathways at a Cu loading of 0.037%, which is equivalent to 3.7% of the total metal loading). This is in keeping with previous works, which demonstrated a deleterious effect on performance with the introduction of high loadings of Cu into precious metal nanoparticles [48,50] and suggested a high sensitivity towards tertiary metal content. While the evaluation of catalytic activity towards H_2O_2 synthesis alone (Figure 3A) may suggest that there is very little difference in the performance over a range of Cu loadings (H_2O_2 synthesis rates between 111 and 116 $mol_{H_2O_2}kg_{cat}^{-1}h^{-1}$ observed for Cu loadings of 0.012–0.025 wt.%), the determination of H_2 conversion rates and H_2O_2 selectivity indicates that a substantial reduction in catalytic selectivity towards H_2O_2 coincides with the introduction of Cu (Figure 3B), which would align with determination of trends in H_2O_2 degradation activity (Figure 3A). Indeed, these observations imply that the enhanced activity of the Cu-containing catalysts is associated with increased reactivity (i.e., the rate of H_2 conversion) rather than H_2O_2 selectivity. However, it is important to consider that such evaluations are not made at comparable rates of H_2 conversion and, notably, the high H_2 selectivity of the 1%AuPd$_{(1.00)}$/ZSM-5 catalyst (81%) can be related to the low rates of conversion (10%) observed. With the introduction of Cu at concentrations greater than 0.025 wt.%, a substantial decrease in H_2 conversion rates was observed, which correlates well with the observed loss in catalytic activity towards both the direct synthesis and subsequent degradation of H_2O_2.

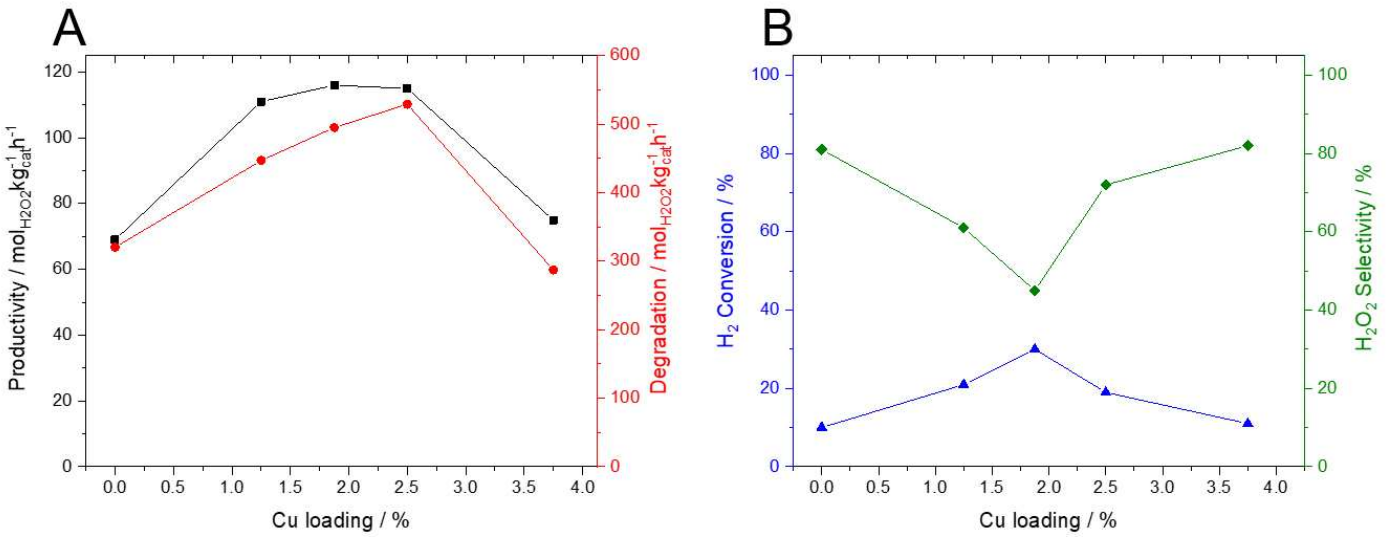

Figure 3. The effect of Cu incorporation into 1%AuPd$_{(1.00)}$/ZSM-5 on catalytic activity. (**A**) Comparison of activity towards the direct synthesis and subsequent degradation of H_2O_2. (**B**) Evaluation of H_2 conversion and selectivity towards H_2O_2 during the H_2O_2 synthesis reaction. ***Key:*** H_2O_2 synthesis (*black squares*); H_2O_2 degradation (*red circles*); H_2 conversion during H_2O_2 direct synthesis reaction (*blue triangles*); H_2O_2 selectivity during H_2O_2 direct synthesis reaction (*green diamonds*). **H_2O_2 direct synthesis reaction conditions:** catalyst (0.01 g), H_2O (2.9 g), MeOH (5.6 g), 5% H_2/CO_2 (420 psi), 25% O_2/CO_2 (160 psi), 0.5 h, 2 °C, and 1200 rpm. **H_2O_2 degradation reaction conditions:** catalyst (0.01 g), H_2O_2 (50 wt.% 0.68 g) H_2O (2.22 g), MeOH (5.6 g), 5% H_2/CO_2 (420 psi), 0.5 h, 2 °C, and 1200 rpm.

With our XPS analysis revealing a modification in the Pd oxidation state as a result of the incorporation of dopant metals (Figure 2), we were subsequently motivated to investigate the 1%AuPdCu/ZSM-5 catalytic series via CO-DRIFTS (Figure 4). CO-DRIFTS is a technique that has been extensively utilised to probe the surface of supported precious metal catalysts [51–54]. For each catalyst, spectra were measured in the 1750–2150 cm^{-1} range, which contains the stretching modes associated with the CO adsorbed on Pd and Au surfaces. The DRIFTS spectra of all the catalysts were dominated by Pd–CO bands. The peak observed at approximately 2080 cm^{-1} represents the CO bound in a linear manner to low co-ordination Pd sites (i.e., corner or edge sites), while the broad feature, centred around 1950 cm^{-1}, represents the bi- and tri-dentate bridging modes of CO on Pd [55]. Upon the introduction of small concentrations of Cu into the AuPd nanoalloy, a small blue shift in the band relates to the linearly bonded CO on Pd, which can be observed. This aligns well with previous investigations by Wilson et al. into the formation of AuPd alloys [51]. In particular, such a shift can be attributed to the segregation of Pd at the nanoparticle surface and a corresponding occupation of lower coordination sites. It is, therefore, possible to propose that the introduction of Cu into AuPd nanoalloys at low concentrations results in a similar modification of the nanoparticle composition.

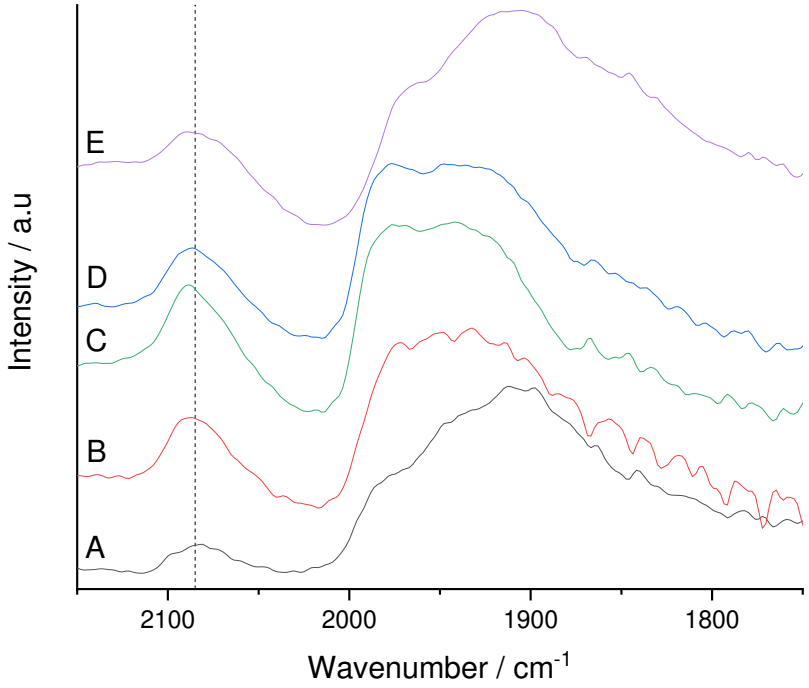

Figure 4. CO-DRIFTS spectra for the as-prepared $1\%AuPd_{(1-X)}Cu_{(X)}/ZSM\text{-}5$ catalysts. (**A**) $1\%AuPd_{(1.00)}/ZSM\text{-}5$; (**B**) $1\%AuPd_{(0.875)}Cu_{(0.125)}/ZSM\text{-}5$; (**C**) $1\%AuPd_{(0.8125)}Cu_{(0.1875)}/ZSM\text{-}5$; (**D**) $1\%AuPd_{(0.75)}Cu_{(0.25)}/ZSM\text{-}5$; and (**E**) $1\%AuPd_{(0.625)}Cu_{(0.375)}/ZSM\text{-}5$.

With the evident improvement upon the incorporation of Cu into a supported $1\%AuPd_{(1.00)}/ZSM\text{-}5$ catalyst, we subsequently set out to further contrast the catalytic performance of the optimal catalyst and the bimetallic AuPd analogue. Time-on-line studies comparing H_2O_2 synthesis rates are reported in Figure 5A, where a significant difference in catalytic performance is observed. Indeed, the enhanced reactivity of the $1\%AuPd_{(0.975)}Cu_{(0.025)}/ZSM\text{-}5$ catalyst is clear, achieving H_2O_2 concentrations (0.35 wt.%) far greater than that of the AuPd analogue (0.21 wt.%) over a 1 h H_2O_2 synthesis reaction. Further investigation of catalytic performance over several successive H_2O_2 synthesis reactions can be seen in Figure 5B, where a marked enhancement in H_2O_2 concentration can be observed over the $1\%AuPd_{(0.975)}Cu_{(0.025)}/ZSM\text{-}5$ catalyst (0.60 wt.%) compared to that achieved by the $1\%AuPd_{(1.00)}/ZSM\text{-}5$ catalyst (0.27 wt.%). Notably, the concen-

tration of H_2O_2 achieved over the AuPdCu catalyst was found to be comparable to that achieved when utilising identical concentrations of Pt as a catalytic promoter for AuPd nanoalloys [44].

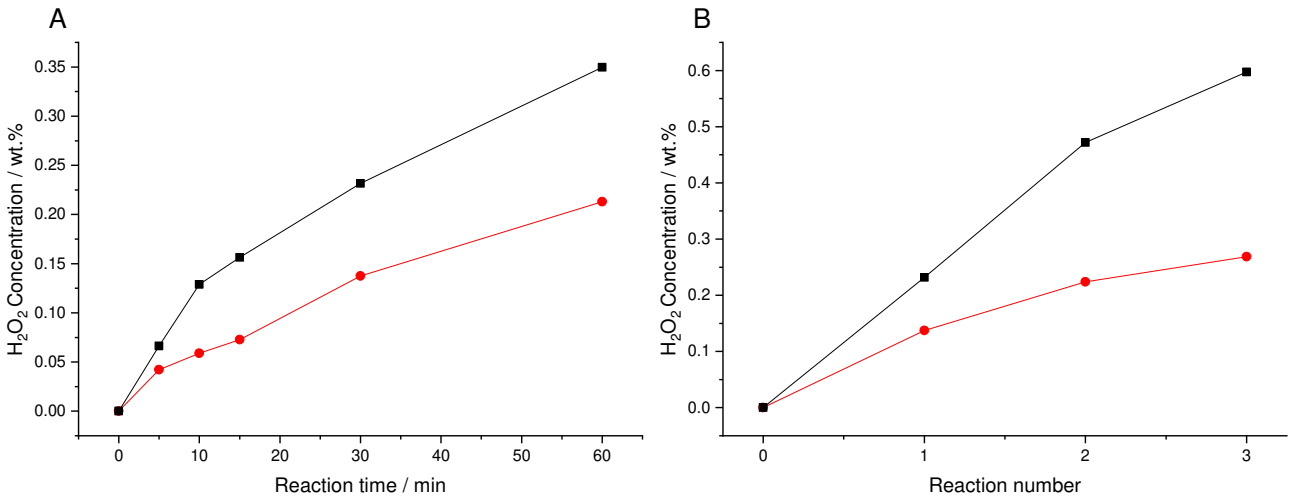

Figure 5. Comparison of catalytic activity towards the direct synthesis of H_2O_2 as (**A**) a function of reaction time and (**B**) over sequential H_2O_2 synthesis reactions. ***Key:*** 1%$AuPd_{(1.00)}$/ZSM-5 (*red circles*) and 1%$AuPd_{(0.975)}Cu_{(0.025)}$/ZSM-5 (*black squares*). **H_2O_2 direct synthesis reaction conditions:** catalyst (0.01 g), H_2O (2.9 g), MeOH (5.6 g), 5% H_2/CO_2 (420 psi), 25% O_2/CO_2 (160 psi), 0.5 h, 2 °C, and 1200 rpm.

Numerous works have elucidated the dependence between catalytic performance towards H_2O_2 synthesis and particle size, with studies by Tian et al., in particular, revealing that particle size in the sub-nanometre range is crucial for achieving optimal catalytic performance, at least in the case of monometallic Pd catalysts [56]. Comparisons of the mean particle size of the as-prepared 1%$AuPd_{(1.00)}$/ZSM-5 and 1%$AuPd_{(0.975)}Cu_{(0.025)}$/ZSM-5 catalysts, as determined from the bright field transmission electron micrographs presented in Figure S4, are reported in Table 1 with a negligible variation in particle size observed between the AuPd and optimal AuPdCu catalysts (3.7–4.1 nm). As such, it is possible to conclude that the enhanced catalytic activity towards H_2O_2 synthesis achieved through the introduction of Cu into AuPd nanoparticles is not associated with increased metal dispersion. Rather, it can be considered that the electronic modification of the Pd species is a result of dopant introduction, as indicated by our CO-DRIFTS (Figure 4) and XPS analysis (Figure 2), as well as possible structural changes which were indicated by our CO-DRIFTS analysis (Figure 4)and are responsible for the observed reactivity improvements.

Table 1. Particle size measurements of as-prepared 1%$AuPd_{(1.00)}$/ZSM-5 and 1%$AuPdCu_{(0.025)}$/ZSM-5 catalysts.

Catalyst	Mean Particle Size/nm (Standard Deviation)	Productivity/mol$_{H_2O_2}$ kg$_{cat}^{-1}$ h^{-1} (H_2O_2 Conc./wt.%)
1%$AuPd_{(1.00)}$/ZSM-5	3.7 (1.43)	69 (0.14)
1%$AuPd_{(0.975)}Cu_{(0.025)}$/ZSM-5	4.4 (1.93)	115 (0.23)

H_2O_2 direct synthesis reaction conditions: catalyst (0.01 g), H_2O (2.9 g), MeOH (5.6 g), 5% H_2/CO_2 (420 psi), 25% O_2/CO_2 (160 psi), 0.5 h, 2 °C, and 1200 rpm.

For any heterogeneous catalyst operating in a liquid phase reaction, the possibility of catalyst deactivation via the leaching of supported metals and the resultant homogeneous contribution to the observed catalytic activity is a major concern. This is particularly true given the ability of colloidal Pd to catalyse the direct synthesis reaction [57]. It was found

that for both the AuPd and AuPdCu catalysts, catalytic activity toward H_2O_2 production decreased upon second use (Table 2). However, the ICP-MS analysis of H_2O_2 reaction solutions (Table 2) and TEM analysis of spent materials (Figure S4) indicated that such a loss in catalyst performance could not be attributed to either the leaching of active metals or nanoparticle agglomeration, with negligible levels of active metals detected through the analysis of H_2O_2 synthesis reaction solutions and the mean particle size determined to be comparable for both the as-prepared and used materials.

Table 2. Catalyst reusability in the direct synthesis and subsequent degradation of H_2O_2.

Catalyst	Productivity/ $mol_{H_2O_2} kg_{cat}^{-1} h^{-1}$		Initial Reaction Rate/ $mmol_{H_2O_2} mmol_{metal}^{-1} h^{-1}$		Degradation/ $mol_{H_2O_2} kg_{cat}^{-1} h^{-1}$		Metal Leached/%		
	Fresh	Used	Fresh	Used	Fresh	Used	Au	Pd	Cu
$1\%AuPd_{(1.00))}/ZSM\text{-}5$	69	57	37.6	27.0	320	397	0	0.17	-
$1\%AuPd_{(0.975)}Cu_{(0.025)}/ZSM\text{-}5$	115	64	48.5	27.1	529	231	0	0.13	BDL

H_2O_2 direct synthesis reaction conditions: catalyst (0.01 g), H_2O (2.9 g), MeOH (5.6 g), 5% H_2/CO_2 (420 psi), 25% O_2/CO_2 (160 psi), 0.5 h, 2 °C, and 1200 rpm. **H_2O_2 degradation reaction conditions:** catalyst (0.01 g), H_2O_2 (50 wt.% 0.68 g) H_2O (2.22 g), MeOH (5.6 g), 5% H_2/CO_2 (420 psi), 0.5 h, 2 °C, and 1200 rpm. BDL: Below detection limits. **Note:** Initial reaction rates were determined after a reaction time of 0.083 h and were calculated based on theoretical metal loading. Metal leaching is presented as a percentage loss of the nominal metal loading of the fresh materials, with the observed levels of leached metal equivalent to approximately 0.002 wt.%.

Similar observations have been recently reported for AuPd-supported catalysts prepared by an identical excess-chloride impregnation procedure, with the loss in catalytic performance upon use found to be associated with a significant loss of surface Cl species, a known promoter of activity in the H_2O_2 synthesis reaction [21]. With these earlier observations in mind, we set out to determine the extent of surface Cl loss (if any) after use in the H_2O_2 direct synthesis reaction via XPS (Figure S5). Interestingly, negligible concentrations of Cl species were observed in either the fresh or used AuPd and AuPdCu catalysts. This is in stark contrast to our earlier investigations into $AuPd/TiO_2$ catalysts prepared via an analogous synthesis technique and possibly highlights the key role of the support in retaining halide species [21]. Regardless, such an observation excludes the possibility of Cl loss as the cause for the observed loss in catalytic performance upon reuse. However, further investigation by XPS (Figures S6 and S7) does reveal a modification in the Au: Pd ratio for both catalysts after use, which may be indicative of nanoalloy restructuring and perhaps, more importantly, a total shift in the Pd speciation towards Pd^0, which can be attributed to the presence of H_2 within the reaction. As such, it is possible to conclude that while the catalytic materials developed within this work represent a promising basis for future study, there is still a need to address stability concerns, particularly around Pd speciation.

4. Conclusions

The introduction of low concentrations of earth-abundant metals (Ni, Cu, Zn) into supported AuPd nanoparticles has been demonstrated to improve catalytic activity towards the direct synthesis of H_2O_2, with the inclusion of Cu in particular, found to offer an enhancement compared to that previously reported upon the use of Pt as a promoter for AuPd nanoalloys. Indeed, the activity of the optimal AuPdCu catalyst is shown to outperform the bimetallic analogue by a factor of 1.7. The underlying cause for the increase in H_2O_2 synthesis activity can be attributed to the electronic modification of the Pd species and changes in the surface composition of the nanoalloys as a result of Cu inclusion, as evidenced by XPS and CO-DRIFTS investigations. While catalytic stability is of concern, with deactivation attributed to in situ reductions in Pd species, it can be considered that these materials represent a promising basis for future exploration in a range of reactions, particularly where the in situ supply of H_2O_2 is required.

Supplementary Materials: The following supporting information can be downloaded at: https://www.mdpi.com/article/10.3390/catal12111396/s1. Table S1. Synthesis details of the precursors used in the preparation of key bi- and tri-metallic 1%AuPd/ZSM-5 catalysts. Table S2. Summary of porosity and surface area of key 1%$AuPd_{(0.0975)}X_{(0.025)}$/ZSM-5 catalysts and HZSM-5(30). Table S3. Comparison of initial H_2O_2 synthesis rates over 1%$AuPd_{(0.0975)}X_{(0.025)}$/ZSM-5 (X = Cu, Ni, Zn) catalysts, as a function of Cu loading. Table S4. The effect of tertiary metal introduction upon the surface atomic composition of 1%$AuPd_{(0.975)}X_{(0.025)}$/ZSM-5 catalysts (X = Cu, Ni, Zn), as determined by XPS. Table S5. Comparison of initial H_2O_2 synthesis rates over 1%AuPdCu/ZSM-5 catalysts, as a function of Cu loading. Figure S1. X-ray diffractograms of 1%$AuPd_{(0.0975)}X_{(0.025)}$/ZSM-5 catalysts. (A) ZSM-5, (B) 1%$AuPd_{(1.00)}$/ZSM-5, (C) 1%$AuPd_{(0.0975)}Cu_{(0.025)}$/ZSM-5, (D) 1%$AuPd_{(0.0975)}Ni_{(0.025)}$/ZSM-5 and (E) 1%$AuPd_{(0.0975)}Zn_{(0.025)}$/ZSM-5. Figure S2. Fourier-transform infrared spectroscopy of 1%$AuPd_{(0.975)}X_{(0.025)}$/ZSM-5 catalysts. (A) ZSM-5, (B) 1%$AuPd_{(1.00)}$/ZSM-5, (C) 1%$AuPd_{(0.975)}Cu_{(0.025)}$/ZSM-5, (D) 1%$AuPd_{(0.975)}Ni_{(0.025)}$/ZSM-5 and (E) 1%$AuPd_{(0.975)}Zn_{(0.025)}$/ZSM-5. Figure S3. BET analysis plots for key 1%$AuPd_{(0.0975)}X_{(0.025)}$/ZSM-5 catalysts and HZSM-5(30). *Key:* ZSM-5(30) (*red triangles*), 1%$AuPd_{(1.00)}$/ZSM-5 (*blue squares*), 1%$AuPd_{(0.975)}Cu_{(0.025)}$/ZSM-5 (*green circles*). Note: ZSM-5 support exposed to calcination prior to metal immobilisation (flowing air, 550 °C, 3 h, 20 °Cmin^{-1}). Figure S4. Representative bright field transmission electron micrographs and corresponding particle size histograms of as-prepared (A) 1%$AuPd_{(1.00)}$/ZSM-5 and (C) 1%$AuPd_{(0.975)}Cu_{(0.025)}$/ZSM-5 catalysts and analogous (B) 1%$AuPd_{(1.00)}$/ZSM-5 and (D) 1%$AuPd_{(0.975)}Cu_{(0.025)}$/ZSM-5 samples after use in the direct synthesis reaction. H_2O_2 direct synthesis reaction conditions: Catalyst (0.01 g), H_2O (2.9 g), MeOH (5.6 g), 5% H_2/CO_2 (420 psi), 25% O_2/CO_2 (160 psi), 0.5 h, 2° C, 1200 rpm. Figure S5. Comparison of surface atomic Cl content of the as-prepared (A) and (B) used 1%$AuPd_{(1.00)}$/ZSM-5 catalyst and the fresh (C) and (D) used 1%$AuPd_{(0.975)}Cu_{(0.025)}$/ZSM-5 analogue. Note: No signal is observed for any catalyst formulation within the expected energy window for Cl(2p) (approx. 200 eV). Figure S6. XPS spectra of Pd(3d) regions for the (A) as-prepared and (B) used 1%$AuPd_{(1.00)}$/ZSM-5 catalyst, after use in the H_2O_2 direct synthesis reaction. *Key:* Au(4d) (green), Pd^0(blue), Pd^{2+}(purple), Ca^{2+} (orange). Figure S7. XPS spectra of Pd(3d) regions for the (A) as-prepared and (B) used 1%$AuPd_{(0.975)}Cu_{(0.025)}$/ZSM-5 catalyst, after use in the H_2O_2 direct synthesis reaction. *Key:* Au(4d) (green), Pd^0(blue), Pd^{2+}(purple), Ca^{2+} (orange).

Author Contributions: A.B. and R.J.L. conducted catalytic synthesis, testing, and data analysis. A.B., R.J.L., D.J.M., and T.E.D. conducted catalyst characterisation and corresponding data processing. R.J.L. and G.J.H. contributed to the design of the study and provided technical advice and result interpretation. R.J.L. wrote the manuscript and Supplementary Information, with all authors commented on and amended both documents. All authors discussed and contributed to the work. All authors have read and agreed to the published version of the manuscript.

Funding: The authors gratefully acknowledge Cardiff University and the Max Planck Centre for Fundamental Heterogeneous Catalysis (FUNCAT) for financial support.

Data Availability Statement: The data presented in this study are fully available within the manuscript and supporting information.

Acknowledgments: The authors would like to thank the CCI-Electron Microscopy Facility which has been part-funded by the European Regional Development Fund through the Welsh Government, and The Wolfson Foundation. XPS data collection was performed at the EPSRC National Facility for XPS ('HarwellXPS'), operated by Cardiff University and UCL, under contract No. PR16195.

Conflicts of Interest: The authors declare no conflict of interest.

References

1. Lewis, R.J.; Hutchings, G.J. Recent Advances in the Direct Synthesis of H_2O_2. *ChemCatChem* **2019**, *11*, 298–308. [CrossRef]
2. Campos-Martin, J.M.; Blanco-Brieva, G.; Fierro, J.L. Hydrogen peroxide synthesis: An outlook beyond the anthraquinone process. *Angew. Chem. Int. Ed.* **2006**, *45*, 6962–6984. [CrossRef]
3. Blaser, B.; Karl-Heinz, W.; Schiefer, J. (Henkel AG and Co KGaA), Stabilizing Agent for Peroxy-Compounds and Their Solutions. U.S. Patent 3122417A, 3 June 1959.
4. Gao, G.; Tian, Y.; Gong, X.; Pan, Z.; Yong, K.; Zong, B. Advances in the production technology of hydrogen peroxide. *Chin. J. Catal.* **2020**, *41*, 1039–1047. [CrossRef]

5. Lewis, R.J.; Ueura, K.; Liu, X.; Fukuta, Y.; Davies, T.E.; Morgan, D.J.; Chen, L.; Qi, J.; Singleton, J.; Edwards, J.K.; et al. Highly efficient catalytic production of oximes from ketones using in situ generated H_2O_2. *Science* **2022**, *376*, 615–620. [CrossRef] [PubMed]
6. Crombie, C.M.; Lewis, R.J.; Kovačič, D.; Morgan, D.J.; Slater, T.J.A.; Davies, T.E.; Edwards, J.K.; Skjøth-Rasmussen, M.S.; Hutchings, G.J. The Influence of Reaction Conditions on the Oxidation of Cyclohexane via the in-situ Production of H_2O_2. *Catal. Lett.* **2021**, *151*, 164–171. [CrossRef]
7. Jin, Z.; Wang, L.; Zuidema, E.; Mondal, K.; Zhang, M.; Zhang, J.; Wang, C.; Meng, X.; Yang, H.; Mesters, C.; et al. Hydrophobic zeolite modification for in situ peroxide formation in methane oxidation to methanol. *Science* **2020**, *367*, 193–197. [CrossRef]
8. Ford, D.C.; Nilekar, A.U.; Xu, Y.; Mavrikakis, M. Partial and complete reduction of O_2 by hydrogen on transition metal surfaces. *Surf. Sci.* **2010**, *604*, 1565–1575. [CrossRef]
9. Voloshin, Y.; Halder, R.; Lawal, A. Kinetics of hydrogen peroxide synthesis by direct combination of H_2 and O_2 in a microreactor. *Catal. Today* **2007**, *125*, 40–47. [CrossRef]
10. Wilson, N.M.; Flaherty, D.W. Mechanism for the Direct Synthesis of H_2O_2 on Pd Clusters: Heterolytic Reaction Pathways at the Liquid–Solid Interface. *J. Am. Chem. Soc.* **2016**, *138*, 574. [CrossRef]
11. Adams, J.S.; Chemburkar, A.; Priyadarshini, P.; Ricciardulli, T.; Lu, Y.; Maliekkal, V.; Sampath, A.; Winikoff, S.; Karim, A.M.; Neurock, M.; et al. Solvent molecules form surface redox mediators in situ and cocatalyze O_2 reduction on Pd. *Science* **2021**, *371*, 626–632. [CrossRef]
12. Ricciardulli, T.; Gorthy, S.; Adams, J.S.; Thompson, C.; Karim, A.M.; Neurock, M.; Flaherty, D.W. Effect of Pd Coordination and Isolation on the Catalytic Reduction of O_2 to H_2O_2 over PdAu Bimetallic Nanoparticles. *J. Am. Chem. Soc.* **2021**, *143*, 5445–5464. [CrossRef] [PubMed]
13. Lewis, R.J.; Ntainjua, E.N.; Morgan, D.J.; Davies, T.E.; Carley, A.F.; Freakley, S.J.; Hutchings, G.J. Improving the performance of Pd based catalysts for the direct synthesis of hydrogen peroxide via acid incorporation during catalyst synthesis. *Catal. Commun.* **2021**, *161*, 106358. [CrossRef]
14. Flaherty, D.W. Direct Synthesis of H_2O_2 from H_2 and O_2 on Pd Catalysts: Current Understanding, Outstanding Questions, and Research Needs. *ACS Catal.* **2018**, *8*, 1520–1527. [CrossRef]
15. Selinsek, M.; Deschner, B.J.; Doronkin, D.E.; Sheppard, T.L.; Grunwaldt, J.; Dittmeyer, R. Revealing the Structure and Mechanism of Palladium during Direct Synthesis of Hydrogen Peroxide in Continuous Flow Using Operando Spectroscopy. *ACS Catal.* **2018**, *8*, 2546–2557. [CrossRef]
16. Henkel, H.; Weber, W. (Henkel AG and Co KGaA), Manufacture of Hydrogen Peroxid. U.S. Patent 1,108,752, 25 August 1914.
17. Priyadarshini, P.; Ricciardulli, T.; Adams, J.S.; Yun, Y.S.; Flaherty, D.W. Effects of bromide adsorption on the direct synthesis of H_2O_2 on Pd nanoparticles: Formation rates, selectivities, and apparent barriers at steady-state. *J. Catal.* **2021**, *399*, 24–40. [CrossRef]
18. Pospelova, T.A.; Kobozev, N. *Russ. J. Phys. Chem.* **1961**, *35*, 1192–1197.
19. Wilson, N.M.; Priyadarshini, P.; Kunz, S.; Flaherty, D.W. Direct synthesis of H_2O_2 on Pd and Au_xPd_1 clusters: Understanding the effects of alloying Pd with Au. *J. Catal.* **2018**, *357*, 163–175. [CrossRef]
20. Richards, T.; Lewis, R.J.; Morgan, D.J.; Hutchings, G.J. The Direct Synthesis of Hydrogen Peroxide Over Supported Pd-Based Catalysts: An Investigation into the Role of the Support and Secondary Metal Modifiers. *Catal. Lett.* **2022**, 1–9. [CrossRef]
21. Brehm, J.; Lewis, R.J.; Morgan, D.J.; Davies, T.E.; Hutchings, G.J. The Direct Synthesis of Hydrogen Peroxide over AuPd Nanoparticles: An Investigation into Metal Loading. *Catal. Lett.* **2022**, *152*, 254–262. [CrossRef]
22. Freakley, S.J.; He, Q.; Harrhy, J.H.; Lu, L.; Crole, D.A.; Morgan, D.J.; Ntainjua, E.N.; Edwards, J.K.; Carley, A.F.; Borisevich, A.Y.; et al. Palladium-tin catalysts for the direct synthesis of H_2O_2 with high selectivity. *Science* **2016**, *351*, 965–968. [CrossRef]
23. Wang, S.; Lewis, R.J.; Doronkin, D.E.; Morgan, D.J.; Grunwaldt, J.; Hutchings, G.J.; Behrens, S. The direct synthesis of hydrogen peroxide from H_2 and O_2 using Pd-Ga and Pd-In catalysts. *Catal. Sci. Technol.* **2020**, *10*, 1925–1935. [CrossRef]
24. Crole, D.A.; Underhill, R.; Edwards, J.K.; Shaw, G.; Freakley, S.J.; Hutchings, G.J.; Lewis, R.J. The direct synthesis of hydrogen peroxide from H_2 and O_2 using PdNi/TiO_2 catalysts. *Philos. Trans. R. Soc. A* **2020**, *378*, 20200062. [CrossRef] [PubMed]
25. Crombie, C.M.; Lewis, R.J.; Taylor, R.L.; Morgan, D.J.; Davies, T.E.; Folli, A.; Murphy, D.M.; Edwards, J.K.; Qi, J.; Jiang, H.; et al. Enhanced Selective Oxidation of Benzyl Alcohol via In Situ H_2O_2 Production over Supported Pd-Based Catalysts. *ACS Catal.* **2021**, *11*, 2701–2714. [CrossRef]
26. Cao, K.; Yang, H.; Bai, S.; Xu, Y.; Yang, C.; Wu, Y.; Xie, M.; Cheng, T.; Shao, Q.; Huang, X. Efficient Direct H_2O_2 Synthesis Enabled by PdPb Nanorings via Inhibiting the O–O Bond Cleavage in O_2 and H_2O_2. *ACS Catal.* **2021**, *11*, 1106–1118. [CrossRef]
27. Tian, P.; Xuan, F.; Ding, D.; Sun, Y.; Xu, X.; Li, W.; Si, R.; Xu, J.; Han, Y. Revealing the role of tellurium in palladium-tellurium catalysts for the direct synthesis of hydrogen peroxide. *J. Catal.* **2020**, *385*, 21–29. [CrossRef]
28. Bernardotto, G.; Menegazzo, F.; Pinna, F.; Signoretto, M.; Cruciani, G.; Strukul, G. New Pd–Pt and Pd–Au catalysts for an efficient synthesis of H_2O_2 from H_2 and O_2 under very mild conditions. *Appl. Catal. A* **2009**, *358*, 129–135. [CrossRef]
29. Quon, S.; Jo, D.Y.; Han, G.; Han, S.S.; Seo, M.; Lee, K. Role of Pt atoms on Pd(1 1 1) surface in the direct synthesis of hydrogen peroxide: Nano-catalytic experiments and DFT calculations. *J. Catal.* **2018**, *368*, 237–247. [CrossRef]
30. Deguchi, T.; Yamano, H.; Takenouchi, S.; Iwamoto, M. Enhancement of catalytic activity of Pd-PVP colloid for direct H_2O_2 synthesis from H_2 and O_2 in water with addition of 0.5 atom% Pt or Ir. *Catal. Sci. Technol.* **2018**, *8*, 1002–1015. [CrossRef]

31. Kim, M.; Han, G.; Xiao, X.; Song, J.; Hong, J.; Jung, E.; Kim, H.; Ahn, J.; Han, S.S.; Lee, K.; et al. Anisotropic growth of Pt on Pd nanocube promotes direct synthesis of hydrogen peroxide. *Appl. Surf. Sci.* **2021**, *562*, 150031. [CrossRef]
32. Xu, J.; Ouyang, L.; Da, G.; Song, Q.; Yang, X.; Han, Y. Pt promotional effects on Pd–Pt alloy catalysts for hydrogen peroxide synthesis directly from hydrogen and oxygen. *J. Catal.* **2012**, *285*, 74–82. [CrossRef]
33. Chen, Q.; Beckman, E.J. Direct synthesis of H_2O_2 from O_2 and H_2 over precious metal loaded TS-1 in CO_2. *Green Chem.* **2007**, *9*, 802–808. [CrossRef]
34. Gong, X.; Lewis, R.J.; Zhou, S.; Morgan, D.J.; Davies, T.E.; Liu, X.; Kiely, C.J.; Zong, B.; Hutchings, G.J. Enhanced catalyst selectivity in the direct synthesis of H_2O_2 through Pt incorporation into TiO_2 supported AuPd catalysts. *Catal. Sci. Technol.* **2020**, *10*, 4635–4644. [CrossRef]
35. Lewis, R.J.; Ueura, K.; Fukuta, Y.; Davies, T.E.; Morgan, D.J.; Paris, C.B.; Singleton, J.; Edwards, J.K.; Freakley, S.J.; Yamamoto, Y.; et al. Cyclohexanone ammoximation via in situ H_2O_2 production using TS-1 supported catalysts. *Green Chem.* 2022; *Advance Article*. [CrossRef]
36. Lewis, R.J.; Ueura, K.; Fukuta, Y.; Freakley, S.J.; Kang, L.; Wang, R.; He, Q.; Edwards, J.K.; Morgan, D.J.; Yamamoto, Y.; et al. The Direct Synthesis of H_2O_2 Using TS-1 Supported Catalysts. *ChemCatChem* **2019**, *11*, 1673–1680. [CrossRef]
37. Nguyen, H.V.; Kim, K.Y.; Nam, H.; Lee, S.Y.; Yu, T.; Seo, T.S. Centrifugal microfluidic device for the high-throughput synthesis of Pd@AuPt core–shell nanoparticles to evaluate the performance of hydrogen peroxide generation. *Lab Chip* **2020**, *20*, 3293–3301. [CrossRef]
38. Ham, H.C.; Hwang, G.S.; Han, J.; Nam, S.W.; Lim, T.H. On the Role of Pd Ensembles in Selective H_2O_2 Formation on PdAu Alloys. *J. Phys. Chem. C* **2009**, *113*, 12943–12945. [CrossRef]
39. Li, J.; Ishihara, T.; Yoshizawa, K. Theoretical Revisit of the Direct Synthesis of H_2O_2 on Pd and Au@Pd Surfaces: A Comprehensive Mechanistic Study. *J. Phys. Chem. C* **2011**, *115*, 25359–25367. [CrossRef]
40. Richards, T.; Harrhy, J.H.; Lewis, R.J.; Howe, A.G.R.; Suldecki, G.M.; Folli, A.; Morgan, D.J.; Davies, T.E.; Loveridge, E.J.; Crole, D.A.; et al. A residue-free approach to water disinfection using catalytic in situ generation of reactive oxygen species. *Nat. Catal.* **2021**, *4*, 575–585. [CrossRef]
41. Lewis, R.J.; Bara-Estaun, A.; Agarwal, N.; Freakley, S.J.; Morgan, D.J.; Hutchings, G.J. The Direct Synthesis of H_2O_2 and Selective Oxidation of Methane to Methanol Using HZSM-5 Supported AuPd Catalysts. *Catal. Lett.* **2019**, *149*, 3066–3075. [CrossRef]
42. Kang, J.; Puthiaraj, P.; Ahn, W.; Park, E.D. Direct synthesis of oxygenates via partial oxidation of methane in the presence of O_2 and H_2 over a combination of Fe-ZSM-5 and Pd supported on an acid-functionalized porous polymer. *Appl. Catal. A* **2020**, *602*, 117711. [CrossRef]
43. Lyu, J.; Wei, J.; Niu, L.; Lu, C.; Hu, Y.; Xiang, Y.; Zhang, G.; Zhang, Q.; Ding, C.; Li, X. Highly efficient hydrogen peroxide direct synthesis over a hierarchical TS-1 encapsulated subnano Pd/PdO hybrid. *RSC Adv.* **2019**, *9*, 13398–13402. [CrossRef] [PubMed]
44. Barnes, A.; Lewis, R.J.; Morgan, D.J.; Davies, T.E.; Hutchings, G.J. Enhancing catalytic performance of AuPd catalysts towards the direct synthesis of H_2O_2 through incorporation of base metals. *Catal. Sci. Technol.* **2022**, *12*, 1986–1995. [CrossRef]
45. Santos, A.; Lewis, R.J.; Malta, G.; Howe, A.G.R.; Morgan, D.J.; Hampton, E.; Gaskin, P.; Hutchings, G.J. Direct Synthesis of Hydrogen Peroxide over Au–Pd Supported Nanoparticles under Ambient Conditions. *Int. Eng. Chem. Res.* **2019**, *58*, 12623–12631. [CrossRef]
46. Edwards, J.K.; Thomas, A.; Carley, A.F.; Herzing, A.A.; Kiely, C.J.; Hutchings, G.J. Au–Pd supported nanocrystals as catalysts for the direct synthesis of hydrogen peroxide from H_2 and O_2. *Green Chem.* **2008**, *10*, 388–394. [CrossRef]
47. Xu, F.; Zhao, L.; Zhao, F.; Deng, L.; Hu, L.; Zeng, B. Electrodeposition of AuPdCu Alloy Nanoparticles on a Multi-Walled Carbon Nanotube Coated Glassy Carbon Electrode for the Electrocatalytic Oxidation and Determination of Hydrazine. *Int. J. Electrochem. Sci.* **2014**, *9*, 2832–2847.
48. Ab Rahim, M.H.; Armstrong, R.D.; Hammond, C.; Dimitratos, N.; Freakley, S.J.; Forde, M.M.; Morgan, D.J.; Lalev, G.; Jenkins, R.L.; Lopez-Sanchez, J.A.; et al. Low temperature selective oxidation of methane to methanol using titania supported gold palladium copper catalysts. *Catal. Sci. Technol.* **2016**, *6*, 3410–3418. [CrossRef]
49. Brehm, J.; Lewis, R.J.; Richards, T.; Qin, T.; Morgan, D.J.; Davies, T.E.; Chen, L.; Liu, X.; Hutchings, G.J. Enhancing the Chemo-Enzymatic One-Pot Oxidation of Cyclohexane via In Situ H_2O_2 Production over Supported Pd-Based Catalysts. *ACS Catal.* **2022**, *12*, 11776–11789. [CrossRef]
50. Joshi, A.M.; Delgass, W.N.; Thomson, K.T. Investigation of Gold−Silver, Gold−Copper, and Gold−Palladium Dimers and Trimers for Hydrogen Peroxide Formation from H_2 and O_2. *J. Phys. Chem. C* **2007**, *111*, 7384–7395. [CrossRef]
51. Wilson, A.R.; Sun, K.; Chi, M.; White, R.M.; LeBeau, J.M.; Lamb, H.H.; Wiley, B.J. From Core–Shell to Alloys: The Preparation and Characterization of Solution-Synthesized AuPd Nanoparticle Catalysts. *J. Phys. Chem. C* **2013**, *117*, 17557–17566. [CrossRef]
52. Zhu, B.; Thrimurthulu, G.; Delannoy, L.; Louis, C.; Mottet, C.; Creuze, J.; Legrand, B.; Guesmi, H. Evidence of Pd segregation and stabilization at edges of AuPd nano-clusters in the presence of CO: A combined DFT and DRIFTS study. *J. Catal.* **2013**, *308*, 272–281. [CrossRef]
53. Bollinger, M.A.; Vannice, M.A. A kinetic and DRIFTS study of low-temperature carbon monoxide oxidation over Au—TiO_2 catalysts. *Appl. Catal. B* **1996**, *8*, 417–443. [CrossRef]
54. Marx, S.; Krumeich, F.; Baiker, A. Surface Properties of Supported, Colloid-Derived Gold/Palladium Mono- and Bimetallic Nanoparticles. *J. Phys. Chem. C* **2011**, *115*, 8195. [CrossRef]

55. Carter, J.H.; Althahban, S.; Nowicka, E.; Freakley, S.J.; Morgan, D.J.; Shah, P.M.; Golunski, S.; Kiely, C.J.; Hutchings, G.J. Synergy and Anti-Synergy between Palladium and Gold in Nanoparticles Dispersed on a Reducible Support. *ACS Catal.* **2016**, *6*, 6623–6633. [CrossRef] [PubMed]
56. Tian, P.; Ding, D.; Sun, Y.; Xuan, F.; Xu, X.; Xu, J.; Han, Y. Theoretical study of size effects on the direct synthesis of hydrogen peroxide over palladium catalysts. *J. Catal.* **2019**, *369*, 95. [CrossRef]
57. Dissanayake, D.P.; Lunsford, J.H. Evidence for the Role of Colloidal Palladium in the Catalytic Formation of H_2O_2 from H_2 and O_2. *J. Catal.* **2002**, *206*, 173. [CrossRef]